Advanced nanocomposite Bi_2WO_6@graphene oxide special material: Optical properties and photocatalytic activity for degradation of phenol red

Chu Manh Nhuong[1], Mai Xuan Truong[1], Nguyen Thi Hien Lan[1], Tran Quoc Toan[1], Luu Tuan Nghia[2*]

[1]Thai Nguyen University of Education, 20 Luong Ngoc Quyen, Phan Dinh Phung, Thai Nguyen, Vietnam;
[2]Center for Vocational Education and Continuing Education, Zone 5, Ha Lam, Quang Ninh, Vietnam.
[*]Corresponding author: luutuannghiadhsptn@gmail.com
Received 8 Aug. 2025; Revised 30 Sep. 2025; Accepted 16 Oct. 2025; Published 18 Nov. 2025.
DOI: https://doi.org/10.54939/1859-1043.j.mst.IMBE.2025.102-107

ABSTRACT

In this paper, the photofluorescence emission, energy reflection and diffusion properties, band gap energy, surface charge distribution and magnetic properties of Bi_2WO_6@(0-5)%GO nanoparticles have been further studied. The photoluminescence (PL) spectrum of Bi_2WO_6@(0-5)%GO nanoparticles has strong emission in the blue-red light region (450-713 nm), in which the peaks at 468 and 569 nm correspond to the energy shift in the oxygen vacancy state of Bi_2WO_6. The emission intensity of Bi_2WO_6@5%GO in the 435-525 nm region is lower than that of Bi_2WO_6, which reduces the recombination rate of electrons and holes in the Bi_2WO_6@5%GO hybrid nanocomposite. GO enhanced the energy absorption capacity of Bi_2WO_6@5%GO in the visible region, and the band gap of Bi_2WO_6@(0-5)%GO nanoparticles was in the range of 2.76 - 2.88 eV. Both GO and Bi_2WO_6@(0-5)%GO nanoparticles had negative surface charges ranging from -21.697 mV to -9.124 mV and had small magnetism. The chemical adsorption of phenol red (PR) on the surface of Bi_2WO_6@(0-5)%GO nanoparticles was from 22.25% to 31.96%, following the second-order adsorption kinetic model with a correlation coefficient R^2 of about (0.971–0.992). In particular, Bi_2WO_6@(0-5)%GO nanoparticles had good photocatalytic activity, the photodegradation efficiency of PR reached 64.89% - 86.04% under visible light illumination in 210 min. The PR photolysis reaction followed the first-order reaction kinetic model, in which the Bi_2WO_6@5%GO nanocomposite exhibited high photocatalytic activity, with the photolysis reaction rate constant 1.83 times larger than that of the original nano Bi_2WO_6. Based on its outstanding properties, nanocomposite Bi_2WO_6@(0-5)%GO has potential applications in the treatment of color indicators/dyes in chemistry and food technology, in the textile industry and in the fields of semiconductor technology, electrical engineering, electronics, luminescence, automation and green chemistry.

Keywords: Bi_2WO_6@x%GO; Nanocomposite; Optical; Photocatalytic; Phenol red.

1. INTRODUCTION

Bi_2WO_6 materials have attracted significant attention due to their unique structural, electrical, and optical properties [1-5]. At room temperature, Bi_2WO_6 exhibits an orthorhombic Aurivillius-type layered structure (space group $P2_1ab$). Its electrical conductivity depends on oxygen partial pressure: ionic conduction dominates at $1–10^{-1}$ atm, while electronic conduction prevails at lower pressures [6-10]. A major drawback is the fast recombination of photogenerated $e^–$–h^+ pairs, which has been addressed by transition metal doping (RE, Cu, Ag, Au, Ti, Fe,…), forming composites with GO, g-C_3N_4, or biochar, and engineering nanostructures (nanosheets, hollow spheres, microspheres). These strategies significantly improve the photocatalytic activity of Bi_2WO_6 [1, 7-8].

With a bandgap of 2.6–2.9 eV, Bi_2WO_6 is suitable for visible-light-driven applications (425 - 480 nm), including organic pollutant degradation, environmental sensing, and energy conversion [1]. Various composites, such as BWO/GO, BWO/GR, BWO/Bi_2MoO_6, BWO/rGO, and BWO/TiO_2/rGO, have been developed, enhancing adsorption and photocatalytic degradation of

RhB, MB, NO, phenol, Cr(VI), bisphenol A, E. coli, and pathogenic bacteria, as well as supercapacitor performance [2-11]. Noble metal doping (Au, Ag, Cu, Pd, Pt) and coupling with BiOI or $BiPO_4$ further improve light absorption, charge separation, and photocatalytic efficiency.

Previous studies characterized Bi_2WO_6@(0–5)%GO (BWG-x) using XRD, FT-IR, Raman, SEM/TEM, EDS, and BET. FT-IR confirmed characteristic GO and Bi_2WO_6 vibrations, while Raman showed D, G peaks of GO and Bi_2WO_6@5%GO modes (Eg, B1g, A1g). XRD indicated a crystalline structure with slightly increased crystallite size (11.16–15.48 nm). SEM/TEM revealed GO nanosheets and BWG-x aggregates <60 nm, and EDS confirmed uniform O, Bi, W, C distribution. Bi_2WO_6@5%GO exhibited a relatively high surface area (15.77 $m^2 \cdot g^{-1}$) with meso-/micropores, close to type III isotherm [12]. Phenol red (PR, $C_{19}H_{14}O_5S$, 354.39 $g \cdot mol^{-1}$), a pH-sensitive triarylmethane dye containing C=C bonds, benzene rings, –OH and $–SO_3$ groups, is widely used in indicators, cell media, pool testing, food processing, aquaculture, and molecular biology, and was once applied in phenolsulfonphthalein (PSP) tests for renal plasma flow. This work investigates the photoluminescence, reflectance, surface charge, magnetism, and photocatalytic activity of BWG-x for PR degradation.

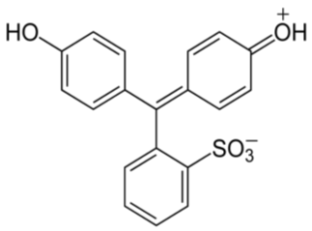

Figure 1. *Ionic structural formula of phenol red.*

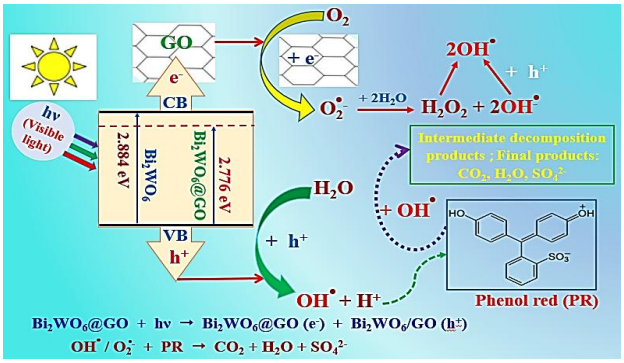

Figure 2. *Photodegradation mechanism of PR by Bi_2WO_6@(0–5)%GO nanocatalysts.*

II. EXPERIMENTAL

2.1. Chemicals, instruments, and equipment

The Bi_2WO_6@(0-5)%GO nanocomposites were synthesized via an ultrasound-assisted hydrothermal method, through 3 steps: (i) precipitation of 0.02 mol $Bi(NO_3)_3 \cdot 5H_2O$ and 0.01 mol $Na_2WO_4 \cdot 2H_2O$; (ii) addition of 0 - 5 wt% GO with stirring (30 °C, 1 h), ultrasonic treatment (60 °C, 2 h), and hydrothermal reaction (200 °C, 15 h); (iii) filtration, washing, drying (60 °C, 2 h), and calcination (400 °C, 3 h). Their optical, surface charge, and magnetic properties, as well as PR degradation ability, were examined using PL (FLS 1000), UV–Vis–DRS (Cary 5000), VSM (VAST), and UV–Vis absorption of PR (UV–1700, Shimadzu) under visible light from a xenon lamp (420 - 575 nm).

2.2. Treatment of phenol red using nanomaterials Bi_2WO_6@GO

For each experiment, 25.0 mg of Bi_2WO_6@(0–5)%GO was added to 50.0 mL PR solution (25.0 mg/L, pH 7.0) in a 100 mL beaker and stirred for 5 min. Adsorption efficiencies were first measured at 15 - 75 min, then the suspensions were irradiated with visible light (0–210 min) at a distance of 10 cm in a dark chamber.

$$\%H = \frac{A_o - A}{A_o}.100 = (1 - \frac{A}{A_o}).100 \quad (1)$$

At selected times, aliquots were withdrawn, centrifuged (3000 rpm, 5 min), and analyzed by UV–Vis (240–660 nm). The PR removal efficiency (%H) was calculated from absorbance at 430

nm using equation (1), where A_0 and A are the absorbance initial and treatment at time *t*. Origin 2025 software was used for data fitting of adsorption and photocatalytic kinetics parameters of Bi_2WO_6@(0–5)%GO nanocomposites.

3. RESULTS AND DISCUSSION

3.1. Optical properties and surface charge distribution of nanoparticles Bi_2WO_6@(0–5)%GO

3.1.1. Photoluminescence emission spectra of the materials

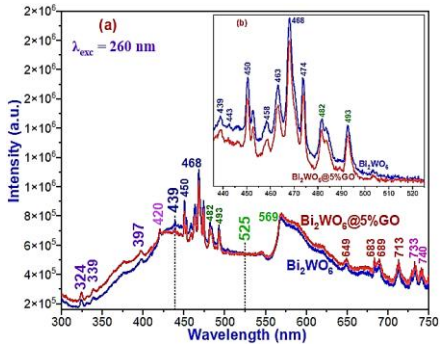

Figure 3. *(a) PL spectra of Bi_2WO_6@(0-5)%GO,(b) Zooming of the range (435 - 525 nm).*

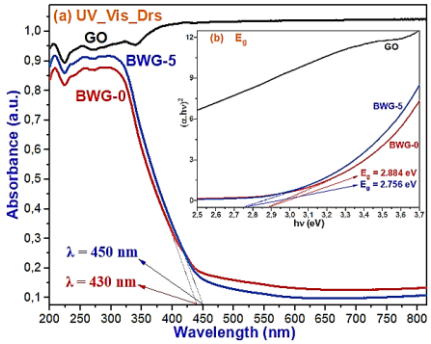

Figure 4. *(a) UV–Vis–DRS and (b) E_g of GO and nanomaterials.Bi_2WO_6@(0–5)%GO.*

Figure 2a shows the PL emission spectra of Bi_2WO_6@(0–5)%GO under 260 nm excitation, with strong emissions from 439–713 nm. The 397 nm peak corresponds to band-edge emission, while peaks at 468 and 569 nm originate from oxygen-vacancy–related states in Bi_2WO_6. Figure 3b highlights the 435–525 nm region, where Bi_2WO_6@5%GO exhibits lower PL intensity than pure Bi_2WO_6. This quenching, caused by GO–Bi_2WO_6 hybridization, indicates suppressed recombination of photogenerated e^-/h^+ pairs and enhanced oxygen-vacancy formation. Emission peaks at 420–544 nm confirm efficient charge separation, suggesting superior photocatalytic performance of Bi_2WO_6@5%GO [2, 3].

Band-edge emission (~ 397 nm) reflects near-band-edge recombination, while peaks at 468 nm (shallow VO/W^{5+} centers) and 525 - 569 nm (deeper V_O or strongly coupled W^{5+} centers) arise from defect states. The broad emissions (439 - 713 nm) indicate multiple trap depths. GO provides electron-accepting pathways, transferring CB electrons from Bi_2WO_6 and reducing radiative recombination. It also promotes V_O formation ($W^{6+} \rightarrow W^{5+}$ reduction), leading to deeper defect emissions (525 - 569 nm, 650 - 713 nm). Shallow V_O acts as a temporary electron reservoir, delaying recombination and enabling interfacial charge transfer to O_2/H_2O for ROS ($^{\bullet}O_2^-$, $^{\bullet}OH$) generation. Thus, GO enhances charge separation and electron transport, improving photocatalytic activity under visible light.

3.1.2. Diffuse reflectance spectra and band gap energy of the materials

UV–Vis–DRS analysis (fig. 3a) shows that while GO absorbs across the full UV–Vis spectrum, the Bi_2WO_6@(0–5)%GO nanocomposites exhibit absorption edges at 430 - 450 nm. Kubelka–Munk plots (fig. 3b) indicate that the band gap (E_g) decreases from 2.884 eV for pristine Bi_2WO_6 to 2.756 eV for Bi_2WO_6@5%GO, consistent with previous studies [1-3, 8-11]. GO incorporation slightly increases crystallite size while narrowing E_g, enhancing photocatalytic performance under visible light.

3.1.3. Zeta potential and magnetic properties of the materials

Surface charge analysis (figure 5) reveals negative zeta potentials (−21.697 to −9.24 mV), suggesting strong adsorption potential toward positively charged pollutants. Magnetic measurements (figure 6) show reduced saturation magnetization in Bi_2WO_6@5%GO due to the non-magnetic nature of GO, confirming successful GO integration. As a result, centrifugation, rather than magnetic separation, is recommended for post-treatment recovery.

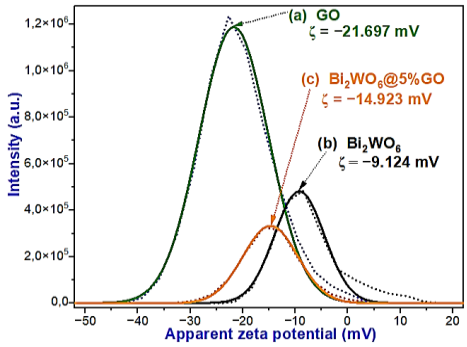

Figure 5. *Zeta potential distribution of: (a) GO, (b) Bi_2WO_6, (c) Bi_2WO_6@5%GO.*

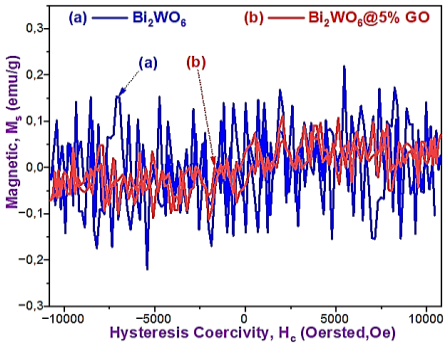

Figure 6. *Magnetic hysteresis curves of: (a) Bi_2WO_6 and (b) Bi_2WO_6@5%GO.*

3.2. Evaluation of the Photocatalytic Activity of Bi_2WO_6@(0–5)%GO Nanocomposites

3.2.1. Effect of treatment time and investigation of adsorption kinetic models

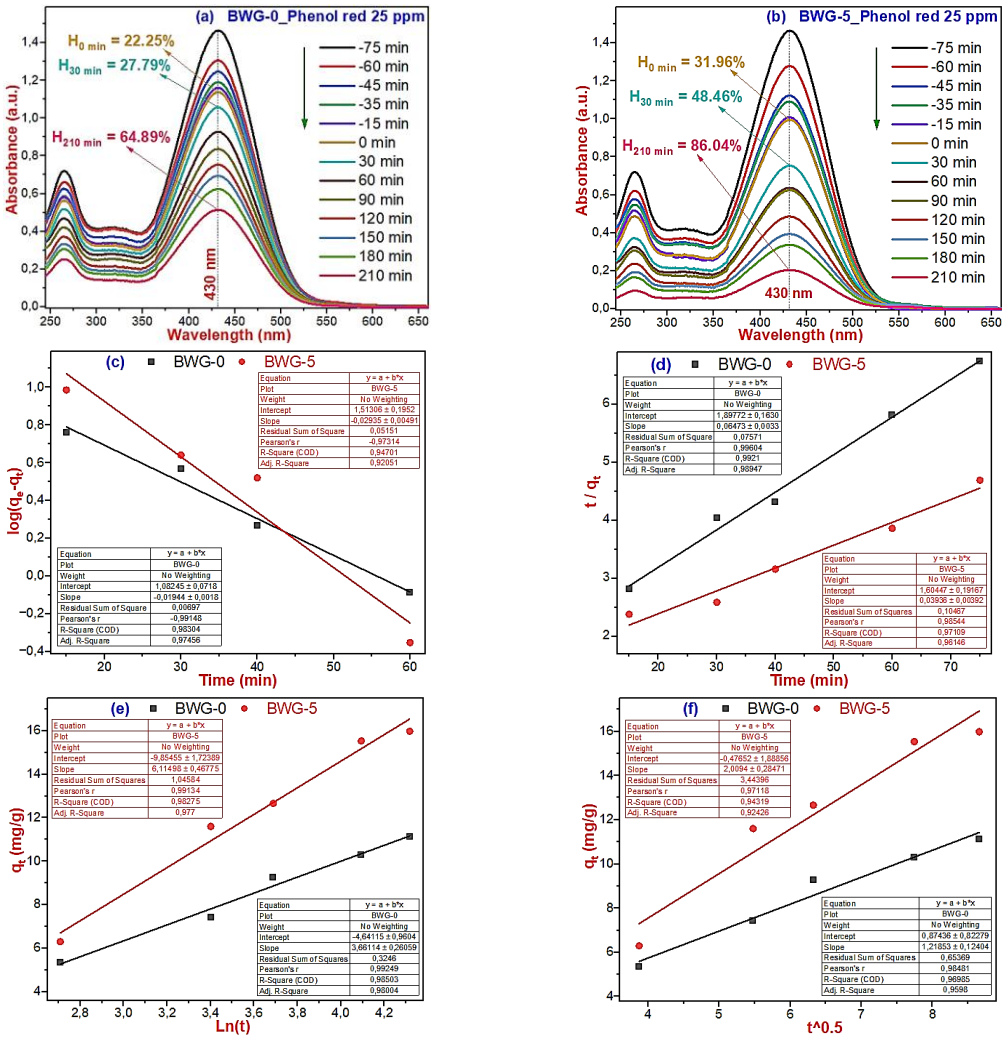

Figure 7. *UV–Vis molecular absorption spectra of PR under visible light in the presence of: (a) Bi_2WO_6; (b) Bi_2WO_6@5%GO, and adsorption kinetic models of PR by Bi_2WO_6@(0–5)%GO nanocomposites: (c) Pseudo-first-order; (d) Pseudo-second-order; (e) Elovich; (f) Intraparticle diffusion.*

Figure 7 (a, b) shows that phenol red (PR) absorbance decreases with time, reaching adsorption equilibrium at 75 minutes, with efficiencies of 22.245–31.964% for Bi_2WO_6@(0–5)%GO nanocomposites. Adsorption kinetics were analyzed using four models (figure 7c–f), among which the pseudo-second-order model fit best (R^2 = 0.971–0.992), outperforming pseudo-first-order, Elovich, and intraparticle diffusion. This indicates that PR adsorption mainly follows a chemisorption mechanism. The pseudo-second-order model yielded maximum adsorption capacities of 9.269–15.240 $mg.g^{-1}$, with rate constants k_2 of 3.68×10^{-3} and 1.61×10^{-3} $g\cdot mg^{-1}\cdot min^{-1}$.

3.2.2. Photocatalytic kinetics of PR degradation using nano Bi_2WO_6@(0-5)%GO

Under visible light (0–210 min), PR concentration decreased with Bi_2WO_6@(0–5)%GO catalysts (figure 7a). Photodegradation efficiency increased from 64.89% (Bi_2WO_6@0%GO) to 86.04% (Bi_2WO_6@5%GO), confirming the positive effect of GO hybridization, which enhances surface area, adsorption, and photocatalytic activity. The Bi_2WO_6@5%GO nanocomposite outperformed BWO/CN (2:1) for MB degradation [11], and adding H_2O_2 can further improve efficiency degradation [1, 4–6]. Its reduced band gap of Bi_2WO_6@5%GO (2.756 eV vs. 2.884 eV for pure Bi_2WO_6, figure 4b) facilitates e^-/h^+ separation, suppresses recombination, and promotes $^{\bullet}O_2^-$ and $^{\bullet}OH$ formation, driving PR redox into CO_2, H_2O, SO_4^{2-} via the mechanism in figure 8.

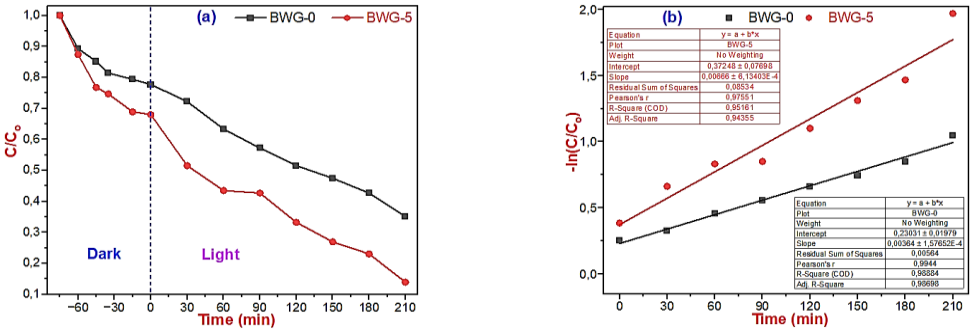

Figure 8. *(a) Variation trend of the C/C_0 ratio of 25 ppm PR solution (at pH 7.0) over treatment time; (b) Linear kinetics of the photocatalytic degradation of PR using Bi_2WO_6@(0–5)%GO nanocatalysts under visible light irradiation.*

Figure 8b shows the first-order kinetics of PR photodegradation with Bi_2WO_6@(0–5)%GO catalysts. The rate constants were 3.64×10^{-3} min^{-1} (0% GO) and 6.66×10^{-3} min^{-1} (5% GO), indicating that Bi_2WO_6@5%GO is 1.83 times more active than pure Bi_2WO_6. Incorporation of GO forms a core–shell structure, where GO thin films increase surface area and promote charge separation, effectively suppressing e^-/h^+ recombination. Consequently, Bi_2WO_6@5%GO shows enhanced photocatalytic efficiency, broadening its potential in organic pollutant treatment [1, 3-6, 9-11] and catalytic disinfection [2, 7, 8].

4. CONCLUSIONS

Compared to pristine Bi_2WO_6, Bi_2WO_6@5%GO nanoparticles show enhanced photoluminescence in the 420–740 nm range, reflecting increased oxygen vacancies. Emission between 435–525 nm indicates efficient separation of photogenerated e^-/h^+ pairs. The Bi_2WO_6@(0–5)%GO nanocomposites possess narrow band gaps (2.88–2.76 eV), suitable for visible-light applications.

All samples carry strongly negative surface charges, enabling high PR adsorption (22.25%–31.96%) via chemisorption, consistent with the pseudo-second-order model. Under visible light, they achieve photocatalytic degradation of PR with efficiencies up to 86.04% after 210 min, following pseudo-first-order kinetics. Importantly, Bi_2WO_6@5%GO exhibits 1.83 times higher photocatalytic activity toward PR than pristine Bi_2WO_6.

REFERENCES

[1]. A. Elaouni *et al.*, "*Bismuth tungstate Bi_2WO_6: a review on structural, photophysical and photocatalytic properties"*. RSC Adv, Vol. 13, pp.17476–17494, (2023).

[2]. C. Chen, *et al.*, *"Adsorption, photocatalytic and sunlight-driven antibacterial activity of Bi_2WO_6/graphene oxide nanoflakes".* Vacuum, Vol. 116, pp. 48-53, (2015).

[3]. C. Sun, *et al.*, *"Sol-gel synthesis of Bi_2WO_6/graphene thin films with enhanced photocatalytic performance for nitric monoxide oxidation under visible light irradiation".* Chemical Physics Letters, Vol. 702, No.2, pp. 49–56, (2018).

[4]. Hadi Salari, *"Facile synthesis of new Z-scheme Bi_2WO_6/Bi_2MoO_6 p–n junction photocatalysts with high photocatalytic activity: Structure, kinetics and mechanism approach".* Materials Research Bulletin, Vol. 131, pp.110979, (2020).

[5]. H. Ma, *et al.*, *"Significant enhanced performance for Rhodamine B, phenol and Cr(VI) removal by Bi_2WO_6 nanocomposites via reduced graphene oxide modification".* Applied Catalysis B: Environmental, Vol. 121–122, pp.198–205, (2012).

[6]. J. Xu, *et al.*, *"A simple method for the preparation of Bi_2WO_6-reduced graphene oxide with enhanced photocatalytic activity under visible light irradiation".* Materials Letters, Vol. 92, pp.126–128, (2013).

[7]. L. Ji, *et al.*, *"Enhanced visible-light-induced photocatalytic disinfection of Escherichia coli by ternary Bi_2WO_6/TiO_2/reduced graphene oxide composite materials: Insight into the underlying mechanism".* Advanced Powder Technology, Vol. 31, pp.128–138, (2020).

[8]. Q. Ma, *et al.*, *"Visible light active graphene oxide modified $Ag/Ag_2O/BiPO_4/Bi_2WO_6$ for photocatalytic removal of organic pollutants and bacteria in wastewater".* Chemosphere, Vol. 306, pp.35512, (2022).

[9]. Z. Li, *et al.*, *"Enhanced Photocatalytic Activity of Hierarchical Bi_2WO_6 Microballs by Modification with Noble Metals".* Catalysts, Vol. 12, pp.130, (2022).

[10]. Z. Mengting, *et al.*, *"2D Graphene oxide (GO) doped p-n type BiOI/Bi_2WO_6 as a novel composite for photodegradation of bisphenol A (BPA) in aqueous solutions under UV-vis irradiation".* Materials Science & Engineering, Vol. 108, pp.110420, (2020).

[11]. O. Rojviroon et al., *"Enhanced photocatalytic activity of Bi_2WO_6/gC_3N_4 nanocomposite in degradation of methylene blue and for energy storage applications".* J. of Molecular Liquids, Vol. 436, 128224 (2025).

[12]. Chu Manh Nhuong et al., *"Thin layer nanocomposite Bi_2WO_6@graphene oxide: unique properties of materials".* Journal of Analytical Sciences, Vol. 31(2A), pp. 61–68, (2025).

TÓM TẮT

Vật liệu đặc chủng nâng cao nanocomposite Bi_2WO_6@graphene oxit: Tính chất quang và hoạt tính quang xúc tác phân hủy phenol đỏ

Bài báo này trình bày kết quả nghiên cứu các tính chất phát xạ huỳnh quang, phản xạ và khuếch tán năng lượng, năng lượng vùng cấm, phân bố điện tích bề mặt và tính chất từ của nanocomposite Bi_2WO_6@(0-5)%GO. Phổ PL của nano Bi_2WO_6@(0-5)%GO phát xạ mạnh trong vùng ánh sáng xanh-đỏ (450 - 713 nm), trong đó các đỉnh phát xạ ở 468 và 569 nm tương ứng với sự dịch chuyển năng lượng trong trạng thái khuyết oxy của Bi_2WO_6. Cường độ phát xạ của Bi_2WO_6@5%GO trong vùng 425-530 nm thấp hơn so với Bi_2WO_6, điều này làm giảm tốc độ tái hợp của electron và lỗ trống trong nanocomposite lai Bi_2WO_6@5%GO. GO làm tăng khả năng hấp thụ năng lượng của vật liệu trong vùng khả kiến và khoảng cách dải của các nanocomposite Bi_2WO_6@(0-5)%GO nằm trong khoảng 2,88 - 2,76 eV. Các nano GO và Bi_2WO_6@(0-5)%GO đều có điện tích bề mặt âm trong khoảng từ -21,697 mV đến -9,124 mV và có độ từ tính nhỏ. Hiệu suất hấp phụ phenol đỏ trên bề mặt các nano Bi_2WO_6@(0-5)%GO đạt từ 22,25% đến 31,96%, theo mô hình động học hấp phụ bậc hai với hệ số tương quan R^2 ~ (0,971 - 0,992). Đặc biệt, các nano Bi_2WO_6@(0-5)%GO có hoạt tính quang xúc tác tốt, hiệu suất quang phân hủy phenol đỏ (PR) đạt 64,89% - 86,04% dưới chiếu sáng khả kiến trong 210 phút. Phản ứng quang phân PR tuân theo mô hình động học bậc nhất, trong đó nanocomposite Bi_2WO_6@5%GO thể hiện hoạt tính quang xúc tác cao, với hằng số tốc độ phản ứng quang phân lớn hơn 1,83 lần so với nano Bi_2WO_6 ban đầu. Dựa trên các đặc tính nổi bật, các hạt nanocomposite Bi_2WO_6@(0-5)%GO có tiềm năng ứng dụng xử lý chất chỉ thị màu/phẩm nhuộm trong hóa học - công nghệ thực phẩm, công nghiệp dệt và trong lĩnh vực công nghệ bán dẫn, kỹ thuật điện, điện tử, phát quang, tự động hóa và hóa học xanh.

Từ khóa: Bi_2WO_6@x%GO; Nanocomposite; Quang học; Quang xúc tác; Phenol đỏ.